Nanoscale

PAPER

View Article Online
View Journal | View Issue

Luminescent iron clusters in solution†

Cite this: *Nanoscale*, 2014, **6**, 1848

Nirmal Goswami,‡[a] Ananya Baksi,‡[b] Anupam Giri,[a] Paulrajpillai Lourdu Xavier,[b] Gautam Basu,[c] Thalappil Pradeep*[b] and Samir Kumar Pal*[a]

Received 30th October 2013
Accepted 26th November 2013

DOI: 10.1039/c3nr05784d

www.rsc.org/nanoscale

Metal clusters, composed of a few atoms at the core, exhibit unique properties and have potential applications. Although atomically precise clusters of noble metals have been synthesized, analogous systems of reactive metals, such as iron, have not been realized in solution due to high reactivity. Here we report the synthesis and characterization of novel iron clusters in the hemoglobin matrix that are highly luminescent (quantum yield 10% at 565 nm). The super-paramagnetic iron clusters, after successful ligand exchange from protein and phase transfer from water to chloroform using tri-octylphosphineoxide (TOPO), were detected as $[Fe_{10}(TOPO)_3(H_2O)_3]^+$, $[Fe_{13}(TOPO)_2(H_2O)]^+$ and $[Fe_8(TOPO)(H_2O)_2]^+$ by mass spectrometry. This study lays the groundwork for exploiting unique properties of soluble iron clusters.

Introduction

Atomically precise metal particles, comprising of only a few atoms with dimensions comparable to the Fermi wavelength of electrons, are called quantum clusters (QCs). The resulting quantum confinement produces unique optical, electronic and chemical properties of QCs that are dramatically different from those of nanoparticles (NPs) which exhibit plasmon absorption. Unusual properties of QCs make them attractive as novel systems of choice for exploring a wide range of phenomena like catalysis, metal ion sensing, and bio-imaging.[1–4] Several monolayer-protected noble metal QCs have been reported to date and a few crystal structures are also known.[5–8] Current research in this area is mostly limited to noble metals, especially Au and Ag, due to their inertness, stability and ease of synthesis. Particularly, QCs of Au (Au_{QCs}) have been well studied because of their unusual stability under ambient conditions and wide spectral tunability, yielding diverse optoelectronic properties.[9–15] Efforts to synthesize atomically precise Ag_{QCs} have been limited due to their higher reactivity.[16,17] Some Ag_{QCs} have also been crystallized.[18] More recently, a growing number of studies have reported Cu_{QCs} and Pt_{QCs}.[19,20] In addition to the nature of the metal, the nature of the ligand can also affect the stability and properties of QCs. Macromolecular templates, where proteins act as ligands, are rather recent entries in the field.[21–23] Several proteins have been used as ligands for such cluster synthesis due to their biocompatibility and high photoluminescence quantum yield of the QCs. The general synthetic route is to first form a metal–protein adduct followed by reduction at elevated pH where the protein acts as the reducing agent or by reduction using an external reducing agent and confining the newly formed cluster core by the protein scaffold simultaneously. These highly luminescent protein-protected clusters are being used as sensors for environmentally hazardous metal ions and other sensitive molecules such as explosives. A number of groups have used protein-protected luminescent QCs in biolabeling.[24,25] It is anticipated that noble metal QCs would be less toxic and more suitable as carriers of biological cargo.[26] However, therapeutic studies have shown that they may not be completely free of side effects.[27] For this field to evolve, it is imperative that novel QCs be explored with characteristics of noble metal QCs but with better biocompatibility and newer properties. Apart from being better biocompatible and cheaper, unique catalytic and magnetic properties of Fe make Fe_{QCs} important candidates among the yet to be explored QCs. Since the first example of metallic Fe NPs (~100 nm),[28] several attempts have been made to characterize them.[29–31] Although recipes to synthesize metallic Fe NPs in the 3–100 nm window exist, new approaches are required for synthesizing Fe_{QCs}. Nanometer sized Fe^0 inherently suffers from instability because of easy surface oxidation upon exposure to air and in the presence of water, making the synthesis of Fe-clusters difficult. Nevertheless, it is important to note that Fe-clusters are known in the gas phase.[32–35] Obviously, suitable chemical procedures and appropriate protection would enable their synthesis in the solution state.

[a]*Department of Chemical, Biological & Macromolecular Sciences, Unit for Nanoscience & Technology, S. N. Bose National Centre for Basic Sciences, Block JD, Sector III, Salt Lake, Kolkata 700098, India. E-mail: skpal@bose.res.in*

[b]*DST Unit of Nanoscience (DST UNS) and Thematic Unit of Excellence (TUE), Department of Chemistry, Indian Institute of Technology Madras, Chennai 600036, India. E-mail: pradeep@iitm.ac.in*

[c]*Department of Biophysics, Bose Institute P 1/12, C. I. T. Road, Scheme VIIM, Kolkata 700054, West Bengal, India*

† Electronic supplementary information (ESI) available. See DOI: 10.1039/c3nr05784d

‡ These authors contributed equally.

Here we describe the first efficient synthesis of highly luminescent and water-soluble Fe_{QCs}, starting from hemoglobin (Hb), a Fe-containing metalloprotein which acts as the iron source as well as the protecting agent. We have employed an efficient ligand exchange strategy with a smaller ligand, trioctyl phosphine oxide (TOPO), and subsequent phase transfer of the cluster from water to chloroform for detailed structural characterization. A number of complementary experimental techniques, including mass spectroscopy, NMR, FT-IR and optical spectroscopy, were used to obtain the precise molecular signature of the clusters in the solution phase. We believe this work will enrich the area further and open a new window to the theoretical as well as the experimental community to understand and evolve this system towards real applications.

Results and discussion

Hemoglobin is a major component of blood that transports oxygen from the respiratory organs (lungs or gills) to the rest of the body. It contains Fe ions, present either as Fe^{2+} or Fe^{3+}, coordinated by four nitrogen atoms of porphyrin present in the protein. In this study, we used Hb as a source of Fe ions as well as the protecting agent to make luminescent Fe_{QCs}. The synthetic approach relies on the extraction of the porphyrin-bound Fe^{2+}/Fe^{3+} in the Hb-matrix using piperidine followed by the reduction of Fe^{2+}/Fe^{3+} with $NaBH_4$ at room temperature (see details in the S1†). After ~12 h of incubation with $NaBH_4$, the solution turned yellowish brown and showed strong yellow luminescence under UV light (Fig. S2†), indicating a change in the oxidation state of the Fe atom in the Hb-matrix. After lyophilization and re-suspension of the product in water, the aqueous solution exhibited the same yellow luminescence under UV light (inset of Fig. 1A). The aqueous phase also showed discrete bands centered at 344 (3.60), 420 (2.95), 507 (2.45) and 639 nm (1.94 eV) (Fig. 1A). Such molecule-like discrete bands are unique to QCs.[36] The absence of any characteristic band corresponding to Fe NPs (at 360 nm) further confirmed that the Fe_{QCs} present in the aqueous phase were nearly pure in the as-synthesized form and were mostly free of large NPs.[31] The Fe_{QCs} showed a luminescence band at 567 nm (2.19 eV) upon photo-excitation at 530 nm (2.34 eV) (Fig. 1A). The quantum yield (QY) of Fe_{QCs} in water (at 565 nm) was determined to be 10%, using Rhodamine 6G (QY = 95% in CH_3CH_2OH) as the reference.

It is well known that the intrinsic fluorescence of proteins, due to aromatic amino acids like tryptophan, can show a tail in the blue region. Furthermore, Hb consists of four porphyrin moieties which are well-known to be red emitting. To rule out potential artifacts, we conducted several control experiments by taking account of all potential products that might have formed after the reaction of $NaBH_4$ and piperidine, in the presence of specific proteins (see Fig. S3–10 and Table S1†). First, we considered apo-myoglobin, as Hb contains four myoglobin units. The observed excitation as well as the emission peaks (Fig. S3†) clearly rule out the possibility of any photoluminescence (PL) due to protein residues peaking at 565 nm. Second, we considered hemato-porphyrin as a prototype of the porphyrin unit present in the protein and performed the same experiment. Upon the treatment of $NaBH_4$ and piperidine, the PL peaks of hemato-porphyrin remained unchanged (Fig. S4†). The observation indicates that the porphyrin moiety is not responsible for the 565 nm PL peak. Finally, hemato-porphyrin was attached to apo-myoglobin as a mimic of Hb (without iron) and treated with $NaBH_4$ and piperidine. Binding of apo-myoglobin with hemato-porphyrin was checked with lifetime measurements (Fig. S9†). The figure indicates that the decay is slower compared to hemato-porphyrin after the treatment. In Fig. S5,† the absence of the 565 nm peak justifies the role of Fe in the yellow luminescence. Our control experiments rule out the possibility of any kind of PL contribution from the protein matrix and support the formation of a new type of material in the protein environment. The occurrence of visible luminescence in a material composed of iron is intriguing. Why should a non-noble metal like Fe show such unique optical properties is still unclear and detailed theoretical studies are needed to establish the precise origin of the optical bands.

Transmission electron microscopic (TEM) images indicated the presence of a large quantity of tiny particles with good uniformity (Fig. 1B). However, conventional HRTEM is not a reliable technique for evaluating the size distribution of QCs due to electron beam-induced coalescence.[37] Although X-ray crystallography is the best method to understand the structure and composition of any material in detail, to date no protein-protected clusters could be crystallized. Mass spectroscopy is a robust technique for characterizing proteins and metal clusters. Matrix-assisted laser desorption ionization mass spectrometry (MALDI MS) and electrospray ionization mass spectrometry (ESI MS) are better suited to study the composition of QCs. MALDI MS of Hb, using DHB as the matrix (details in the ESI†), showed two peaks at m/z 15 230 and 15 990 Da due to the α-globin chain (MW: 15 126.4 Da) and β-globin chain (MW: 15 867.2 Da) of Hb. These peaks were shifted to m/z values 15 760 and 16 500 Da, respectively in the case of Fe_{QCs}@Hb (Fig. 1C) confirming successful cluster formation. This mass difference corresponds to 7–10 Fe atoms and the composition can be roughly assigned to Fe_{7-10}@Hb. However, due to resolution limitations in the higher mass range, the exact number of Fe atoms, determined from the mass difference, may not be correct. This problem was circumvented by a ligand-exchange strategy with a small ligand, tri-octylphosphineoxide (TOPO) (see later in the text). The ligand-exchanged clusters were characterized using ESI MS analysis, a more accurate technique for assigning the composition of molecules containing multiple isotopes.

The oxidation state of Fe was investigated by a number of techniques. X-ray photoelectron spectroscopy (XPS) is the most appropriate method to confirm the oxidation state of the core for atomically precise noble metal clusters. In the present study, although we attempted to obtain the XPS spectrum, due to the inherent poor signal intensity of Fe 2p in XPS as well as the low density of clusters in the protein, we could not establish the oxidation state of Fe in the cluster. Instead, we have performed an indirect method to verify the oxidation state of Fe that we refer to as the "luminal experiment" (details in S1†). Briefly, Hb-bound Fe^{2+}/Fe^{3+} in blood is a catalyst for the

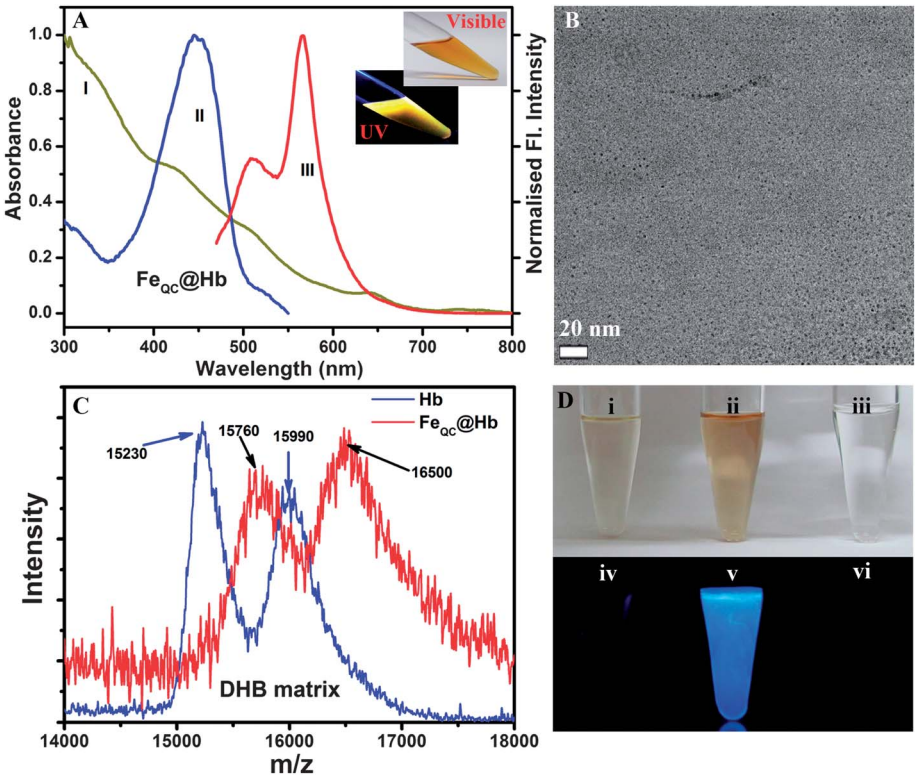

Fig. 1 (A) UV-vis absorption spectrum (yellow) of the water soluble cluster indicates the discrete, molecular like bands. Excitation (blue) and PL (red) spectra of Fe_{QC}@Hb in water where, excitation wavelength = 530 nm and PL wavelength = 565 nm. (B) TEM image of Fe_{QC}@Hb shows a core size of less than 2 nm. Several tiny particles of nearly uniform size are spread over the grid. (C) MALDI-TOF mass spectra of Hb (blue) and Fe_{QC}@Hb (red) in the linear positive mode using the dihydroxybenzoic acid (DHB) matrix. (D) Upper panel: bright field photographs of the luminol–hydrogen peroxide mixture after the addition of (i) Fe_{QC}@Hb (ii) Hb and (iii) water (control). Lower panel: dark field photograph of the luminol–hydrogen peroxide mixture after the addition of (iv) Fe_{QC}@Hb (v) Hb and (vi) water (control). Note that, the chemiluminescence observed for the luminol–hydrogen peroxide mixture (vi) is very poor; however, increases several folds in the presence of Hb (v) because of the presence of Fe^{2+} and Fe^{3+}. In the case of Fe_{QC}@Hb, the solution does not show any chemiluminescence revealing that Fe is in the zero oxidation state.

chemiluminescence reaction that causes luminol to intensely glow blue in the presence of peroxide.[38] During this reaction, Fe^{2+}/Fe^{3+} is reduced with the concomitant oxidation of H_2O_2 to O_2. However, if Fe is already in the 'zero' oxidation state, it cannot catalyze the chemiluminescence reaction. Unlike the case with Hb, Fe_{QC}@Hb could not induce a blue glow in a mixture of luminol and H_2O_2 (Fig. 1D) suggesting that the as-prepared QCs are in the metallic state.

Although water-soluble, protein protected Fe_{QCs} showed evidence of high stability and quantum efficiency, accurate molecular identification by MALDI MS analysis was a major problem. It has been demonstrated that TOPO (tri-octylphosphineoxide) can be used as a stabilizing agent for Fe nanoparticles.[31] Moreover, TOPO can be used for preventing aggregation and slowing down oxidation of the Fe nanoparticles by air.[31] To work in a lower mass range, we chose TOPO, an organic ligand, for ligand exchange as well as for transferring the Fe_{QCs} into chloroform (details in S1†). TOPO-capped Fe_{QCs} (Fe_{QC}@TOPO) in chloroform also exhibited discrete, molecule-like bands at 355 (3.49), 402 (3.09), 516 (2.40), and 570 nm (2.18 eV) (Fig. 2A). The bands were shifted from the corresponding bands of Fe_{QC}@Hb in aqueous medium (Fig. 1A). Note that during ligand exchange, phase transfer was partial which indicated that only a part of the clusters is present in the organic phase. Excitation and photoluminescence (PL) spectra of Fe_{QC}@TOPO in chloroform are shown in Fig. 2B. ^{1}H-NMR experiments showed the chloroform layer, containing TOPO, to be free of Hb or piperidine (Fig. S11†). The presence of tiny Fe_{QCs} in the chloroform layer was verified from TEM images and energy dispersive spectroscopy (Fig. S12†). The clusters aggregated upon long-time electron beam irradiation forming nanoparticles (Fig. S12†), as seen before in the case of Au clusters.[37] Therefore, it is fair to conclude that the 565 nm peak originates solely from Fe_{QC}@TOPO. We note that the PL peak remained constant during phase transfer while the absorption spectra changed. For Au clusters, Negishi *et al.* have shown that when the core size changes from Au_{10} to Au_{18} the lowest energy absorption peak changes from 330 nm to 570 nm, whereas the PL maximum remains constant at 1.5 eV.[13] Akin to the Au clusters, we anticipate that iron clusters with different core sizes present in chloroform could have similar luminescence, however, with different extinction compared to the clusters present in water. The solution of Fe_{QC}@TOPO was brown under visible light but exhibited a bright yellow color when irradiated with UV light (Fig. 2B inset). Using Rhodamine 6G as the reference, the QY of the Fe_{QC}@TOPO was determined to be

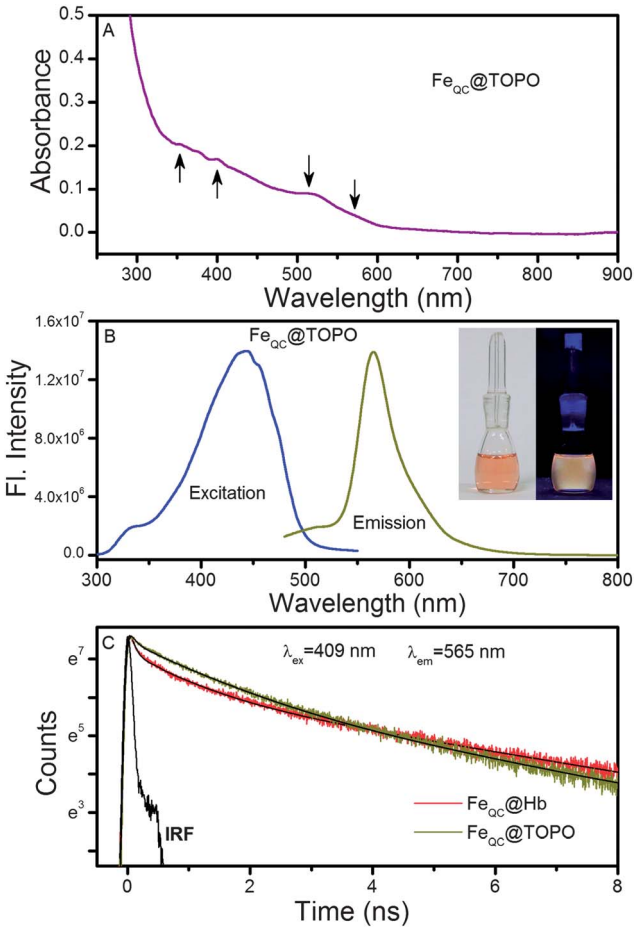

Fig. 2 (A) UV-vis absorption spectrum of Fe$_{QC}$@TOPO in chloroform after solvent correction. Arrows indicate the absorption bands. (B) Excitation and PL spectra of Fe$_{QC}$@TOPO in chloroform solution. Inset shows the photograph of the cluster solution in chloroform under (I) visible and (II) UV light. (C) Photoluminescence decay of Fe$_{QC}$@Hb and Fe$_{QC}$@TOPO with instrument response function (IRF) ~60 ps. Standard error of decay time components is ~10%.

12%. Fig. 2C shows the decay transients of the Fe$_{QCs}$ before and after phase transfer. Luminescence lifetime values of the Fe$_{QCs}$, obtained from luminescence transients observed at 565 nm were 0.08 (64%), 0.91 (22%), and 3.90 (14%) ns in water and 0.11 (43%), 1.14 (38%), and 3.60 (19%) ns in chloroform. The observed differences of the transients are not very significant and probably arise due to reduction of the non-radiative decay in non-polar chloroform.[39] The luminescence transients were found to be almost invariant as a function of excitation wavelengths (375, 409 and 445 nm), which provided strong evidence that the observed clusters have a similar luminescence profile (Fig. S13†).

In order to obtain more definite mass spectral signatures, we performed ESI MS analysis of TOPO capped Fe$_{QCs}$ in 9 : 1 chloroform : acetonitrile in positive ion mode, in the m/z range of 100–4000 Da. TOPO showed an intense peak at m/z 387 due to its molecular ion peak. The TOPO dimer and other fragments were also observable in the lower mass region (m/z < 800). In the region beyond m/z 800, specific peaks due to clusters appear while the lower mass region is dominated by ligand peaks (Fig. 3). In this figure, the expanded cluster region shows the presence of multiple cores namely, $[Fe_8(TOPO)(H_2O)_2]^+$, $[Fe_{10}(TOPO)_3(H_2O)_3]^+$ and $[Fe_{13}(TOPO)_2(H_2O)]^+$. It is to be noted that, unlike several Au clusters,[40] we have not seen any multiply charged species and all the compositions were verified with theoretically calculated isotope patterns. Along with the major peaks observed as discussed above, several small intensity peaks are also visible in the range studied. Most of the peaks are fragments of the above mentioned peaks. One can envisage three different ways of fragmentation, as observed in the present study: (a) direct loss of TOPO, (b) loss of water (one or multiple) molecule, and (c) loss of a TOPO fragment namely, the octyl group. For instance, the peak at m/z 1131 is a TOPO-devoid fragment of $[Fe_{13}(TOPO)_2(H_2O)]^+$. Similarly, the peak at m/z 1386 corresponds to the TOPO-devoid fragment of $[Fe_{10}(TOPO)_3(H_2O)_3]^+$. The m/z 1257 peak is assigned to $[Fe_8(TOPO)_2(H_2O)_2]^+$ and hence, the m/z 870 peak is probably due to $[Fe_8(TOPO)(H_2O)_2]^+$, arising after the loss of one TOPO moiety. These are examples of direct loss of the TOPO moiety from the parent cluster. The fragmentations were ascertained by extensive MS/MS studies (see later). Loss as well as addition of water molecules were also observed in some cases. Two peaks, at m/z 1368 and m/z 1404, accompanying the m/z 1386 peak (assigned to $[Fe_{10}(TOPO)_2(H_2O)_3]^+$), arise due to the loss/gain of one water molecule as $[Fe_{10}(TOPO)_3(H_2O)_2]^+$ and $[Fe_{10}(TOPO)_3(H_2O)_4]^+$ respectively. Water loss was also observed in the case of $[Fe_8(TOPO)_2(H_2O)_2]^+$, where loss of two water molecules and one ligand leads to a bare Fe_8^+ core (see Fig. 4). The peak centered

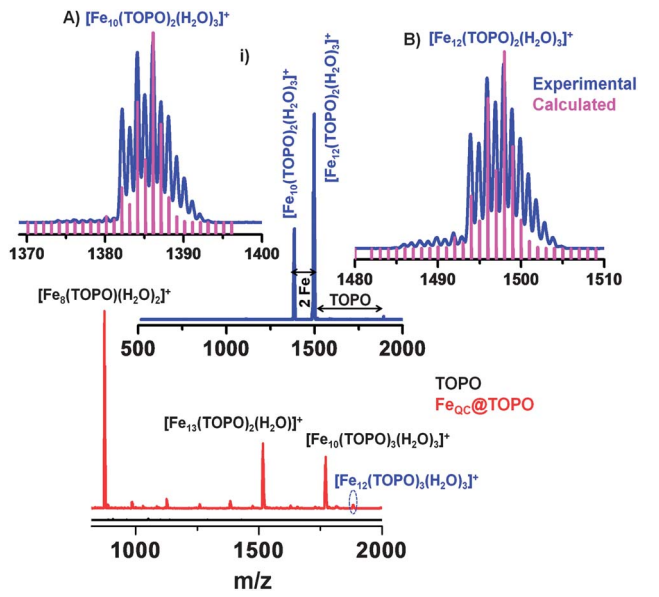

Fig. 3 ESI MS of TOPO and Fe$_{QCs}$@TOPO in the mass range m/z 800–2000 Da showing the presence of $[Fe_8(TOPO)(H_2O)_2]^+$, $[Fe_{10}(TOPO)_3(H_2O)_3]^+$, $[Fe_{12}(TOPO)_3(H_2O)_3]^+$ and $[Fe_{13}(TOPO)_2(H_2O)]^+$. Inset (i) shows MS/MS of $[Fe_{12}(TOPO)_3(H_2O)_3]^+$ where ligand as well as Fe loss is also observable. (A and B) $[Fe_{12}(TOPO)_2(H_2O)_3]^+$ and $[Fe_{10}(TOPO)_2(H_2O)_3]^+$ are compared with the theoretically calculated isotope patterns of these species.

around *m*/*z* 1660 is due to the loss of an octyl group from TOPO from the parent ion $[Fe_{10}(TOPO)_3(H_2O)_3]^+$, which confirms the presence of the third type of fragmentation pattern.

Another kind of fragmentation could be the loss of Fe. This fragmentation pattern is seen for $[Fe_{12}(TOPO)_3(H_2O)_3]^+$. The presence of a Fe_{12} core was confirmed from the MS/MS data, where the parent peak, $[Fe_{12}(TOPO)_3(H_2O)_3]^+$, shows the loss of two Fe atoms yielding $[Fe_{10}(TOPO)_2(H_2O)_3]^+$ along with $[Fe_{12}(TOPO)_2(H_2O)_3]^+$ (Fig. 3i). The same $[Fe_{10}(TOPO)_2(H_2O)_3]^+$ fragment was seen in the MS/MS of $[Fe_{10}(TOPO)_3(H_2O)_3]^+$ (see Fig. 4), where the parent cluster loses one ligand molecule to generate the observed fragment. Fig. 3A and B clearly show that the calculated and the experimentally observed isotope patterns match very well. Although the mass of two Fe atoms and that of one octyl group are nearly identical, the mismatch in the observed isotope pattern in the case of $[Fe_{10}(TOPO)_2(H_2O)_3]^+$ rules out the presence of the octyl group.

Extensive MS/MS studies were performed to understand the cluster compositions. Collision energy dependent MS/MS study of the clusters showed consecutive ligand losses for all the clusters investigated (Fig. S14–S18†). In Fig. 4A, MS/MS data for $[Fe_{10}(TOPO)_3(H_2O)_3]^+$, $[Fe_{12}(TOPO)_3(H_2O)_3]^+$ and $[Fe_{13}(TOPO)_2(H_2O)]^+$ are shown, keeping all experimental parameters and collision energies identical. In all the cases, ligand loss can be seen with good isotope distribution, matching with the calculated spectrum (data for $[Fe_{13}(TOPO)_2(H_2O)]^+$ are shown in Fig. 4B). The presence of Fe was also confirmed by conducting MS/MS on each peak in a given envelope for the isotopes. For example, in the case of $[Fe_{13}(TOPO)_2(H_2O)]^+$, peaks in the range *m*/*z* 1514–1522 Da were chosen with an isotope width of 1 Da and MS/MS was performed (Fig. 4C). Each peak yielded a distribution of peaks that arose principally due to the presence of Fe. For $[Fe_8(TOPO)(H_2O)_2]^+$, ligand as well as water loss could be observed, producing a bare $[Fe_8]^+$ core (Fig. 4D and S17†). The presence of water, bound to the cluster core, was also observed in the MS/MS study for the Fe_{13} core, where, upon higher collision energy, $[Fe_{13}(TOPO)_2(H_2O)]^+$ loses two ligands to yield $[Fe_{13}(H_2O)]^+$ (Fig. S16†). This study proves the presence of attached water to the cluster core, which may act as a ligand. We observed the loss of TOPO in most of the cases, which could be a reason behind the less than expected number of observed ligands attached to the core. It is possible that before we could detect the ion in ESI MS, the cluster might have already lost some ligands which was seen in the case of $[Fe_8(TOPO)_2(H_2O)_2]^+$ (Fig. S18†). Another reason for the discrepancy might be that the steric hindrance due to the presence of three octyl chains

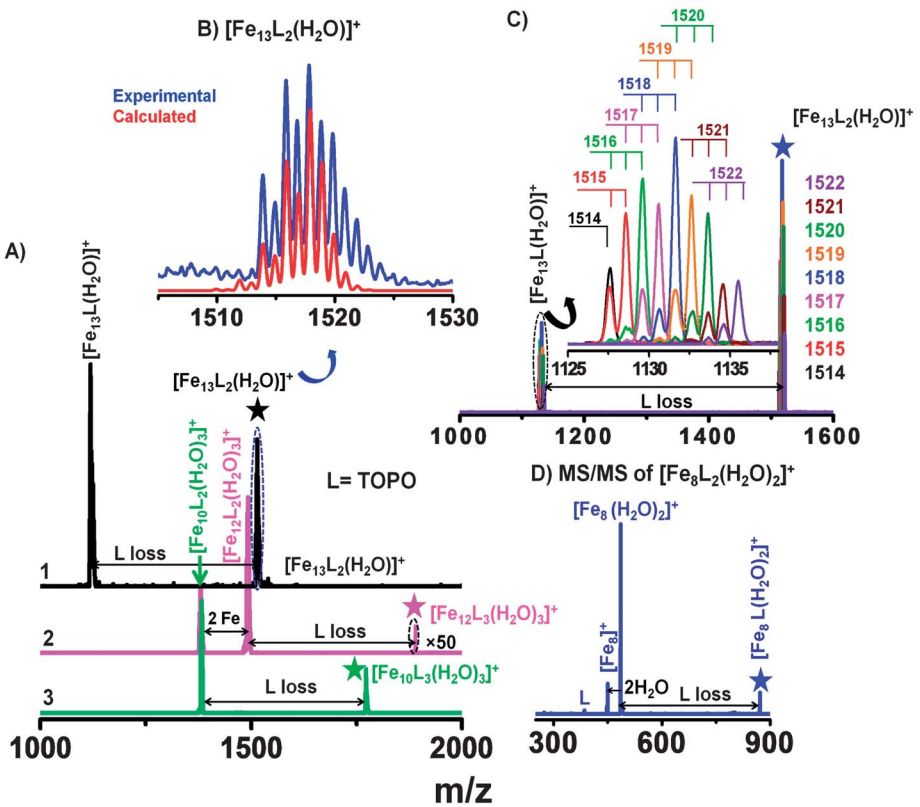

Fig. 4 (A) ESI MS/MS of (1) $[Fe_{13}(TOPO)_2(H_2O)]^+$ (black), (2) $[Fe_{12}(TOPO)_3(H_2O)_3]^+$ (magenta) and (3) $[Fe_{10}(TOPO)_3(H_2O)_3]^+$ (green), showing subsequent ligand losses. For all the cases, parent ions are marked with stars and for fragments, the compositions are indicated. $[Fe_{12}(TOPO)_3(H_2O)_3]^+$ shows two Fe losses also. In this case, the intensity of the parent peak has been multiplied by 50 to make it visible. (B) $[Fe_{13}(TOPO)_2(H_2O)]^+$ spectrum is compared with the calculated spectrum. (C) MS/MS spectra of each peak in the $[Fe_{13}(TOPO)_2(H_2O)]^+$ envelope, with a mass width of 1 Da. Fragment peaks after ligand loss are expanded in the inset, showing isotope distribution, principally due to iron. The parent ion chosen for MS/MS is mentioned above the isotope pattern observed. (D) ESI MS/MS of $[Fe_8(TOPO)_2(H_2O)_2]^+$ showing ligand as well as water losses to give a bare $[Fe_8]^+$ core.

present in a single TOPO molecule acted as a deterrent to attachment of more TOPO ligands. However, only a detailed theoretical study on the position and conformation of the ligands and structure of the cluster core can sort out this puzzle.

Bound water molecules have been reported earlier for dendrimer capped Au_8 nanodots by Dickson *et al.*[41] However, the presence of three water molecules bound to Fe, a metal much more reactive than Au, was totally unexpected. The MS data were complemented by the solid-state FT-IR studies of TOPO and Fe_{QC}@TOPO where it was found that both TOPO and Fe_{QC}@TOPO contain small amounts of water (Fig. S19†). To further probe the nature of water in TOPO and Fe_{QC}@TOPO, ^{1}H NMR studies were performed on TOPO and Fe_{QC}@TOPO in $CDCl_3$. Superimposed ^{1}H-NMR spectra of TOPO and Fe_{QC}@TOPO are shown in Fig. 5. Except for one singlet resonance (2.32 ppm for TOPO and 1.69 ppm for Fe_{QC}@TOPO samples), the two spectra are identical and are in agreement with the previously published spectrum of TOPO.[42] The unique singlet peaks in each spectrum, distinct from pure water signal in chloroform (7.24 ppm), could be attributed to TOPO/Fe_{QC}@TOPO bound water since the peaks disappeared upon addition of D_2O. This is consistent with the presence of bound water molecules associated with Fe_{QC}@TOPO (from ESI MS and FT-IR) and TOPO (from FT-IR). If the water signal in Fe_{QC}@TOPO indeed corresponds to molecules bound to Fe_{QCs}, then the super-paramagnetic Fe_{QC}-center (Fig. S20†) is expected to induce faster relaxation and an upfield chemical shift of the Fe_{QC}-bound water resonance. Compared to that in TOPO, the water signal in Fe_{QC}@TOPO showed an upfield shift (0.63 ppm) and faster relaxation, both in terms of spin-lattice relaxation time $T1$ (2.54 s in TOPO and 1.13 s in Fe_{QC}@TOPO) and line width or $1/T2^*$ (0.019 ppm in TOPO and 0.034 ppm in Fe_{QC}@TOPO). The presence of the upfield shifted and broadened water peak (Fig. 5) in the background of all other proton peaks (due to TOPO) establishes a strong interaction of water molecules on the cluster surface.

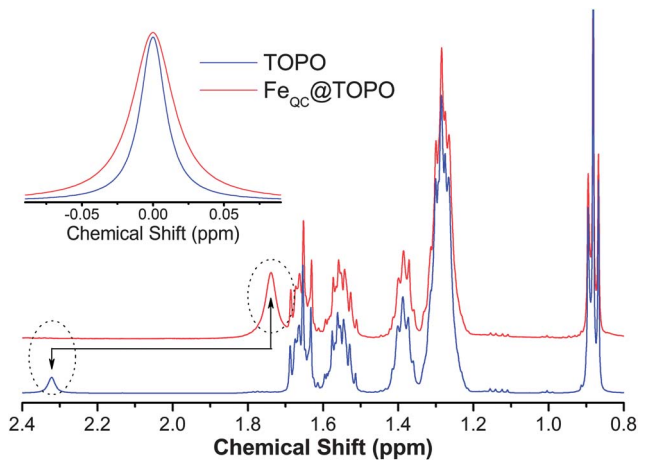

Fig. 5 ^{1}H-NMR spectra of TOPO (blue) and Fe_{QC}@TOPO (red). Bound water resonances for both the samples are marked with dotted circles. Broadening of the Fe_{QC}@TOPO-bound water resonance is shown in the inset.

Conclusion

In summary, we have devised a facile synthetic route for preparing atomically precise and highly luminescent Fe_{QCs}. These clusters synthesized in solution have been detected as $[Fe_8(TOPO)(H_2O)_2]^+$, $[Fe_{10}(TOPO)_3(H_2O)_3]^+$, $[Fe_{12}(TOPO)_2(H_2O)_3]^+$ and $[Fe_{13}(TOPO)_2(H_2O)]^+$, with well-defined and unique isotope distribution in ESI MS. The cluster contains water molecules as revealed by our MS/MS analysis which was corroborated by FT-IR and NMR spectroscopic studies. It is anticipated that a theoretical study will provide further insights into the structure, stability and conformation of the cluster. We believe that this new material holds promise for fundamental applications like catalysis, imaging and sensing.

Acknowledgements

N.G. and A.B thank CSIR, India, for fellowships. A.G. thanks UGC, India, for a fellowship. We thank Mr Barun Majumder for his assistance in NMR experiments. We thank DST for financial grants (DST/TM/SERI/2k11/103 and SB/S1/PC-011/2013). T.P. thanks the Nano Mission of DST, Government of India for constantly supporting his research program.

References

1 N. de Silva, J.-M. Ha, A. Solovyov, M. M. Nigra, I. Ogino, S. W. Yeh, K. A. Durkin and A. Katz, *Nat. Chem.*, 2010, **2**, 1062–1068.
2 Z. Wu, M. Wang, J. Yang, X. Zheng, W. Cai, G. Meng, H. Qian, H. Wang and R. Jin, *Small*, 2012, **8**, 2028–2035.
3 C.-A. J. Lin, T.-Y. Yang, C.-H. Lee, S. H. Huang, R. A. Sperling, M. Zanella, J. K. Li, J.-L. Shen, H.-H. Wang, H.-I. Yeh, W. J. Parak and W. H. Chang, *ACS Nano*, 2009, **3**, 395–401.
4 P. L. Xavier, K. Chaudhari, A. Baksi and T. Pradeep, *Nano Rev.*, 2012, **3**, 14767.
5 M. Zhu, C. M. Aikens, F. J. Hollander, G. C. Schatz and R. Jin, *J. Am. Chem. Soc.*, 2008, **130**, 5883–5885.
6 H. Qian, W. T. Eckenhoff, Y. Zhu, T. Pintauer and R. Jin, *J. Am. Chem. Soc.*, 2010, **132**, 8280–8281.
7 P. D. Jadzinsky, G. Calero, C. J. Ackerson, D. A. Bushnell and R. D. Kornberg, *Science*, 2007, **318**, 430–433.
8 M. W. Heaven, A. Dass, P. S. White, K. M. Holt and R. W. Murray, *J. Am. Chem. Soc.*, 2008, **130**, 3754–3755.
9 A. Dass, *J. Am. Chem. Soc.*, 2009, **131**, 11666–11667.
10 J. Akola, M. Walter, R. L. Whetten, H. Häkkinen and H. Grönbeck, *J. Am. Chem. Soc.*, 2008, **130**, 3756–3757.
11 Z. Y. Li, N. P. Young, M. Di Vece, S. Palomba, R. E. Palmer, A. L. Bleloch, B. C. Curley, R. L. Johnston, J. Jiang and J. Yuan, *Nature*, 2008, **451**, 46–48.
12 I. Dolamic, S. Knoppe, A. Dass and T. Bürgi, *Nat. Commun.*, 2012, **3**, 798.
13 Y. Negishi, K. Nobusada and T. Tsukuda, *J. Am. Chem. Soc.*, 2005, **127**, 5261–5270.
14 R. L. Whetten and R. C. Price, *Science*, 2007, **318**, 407–408.
15 P. R. Nimmala and A. Dass, *J. Am. Chem. Soc.*, 2011, **133**, 9175–9177.

16 H. Xu and K. S. Suslick, *Adv. Mater.*, 2010, **22**, 1078–1082.
17 T. U. B. Rao, B. Nataraju and T. Pradeep, *J. Am. Chem. Soc.*, 2010, **132**, 16304–16307.
18 H. Yang, Y. Wang, H. Huang, L. Gell, L. Lehtovaara, S. Malola, H. Hakkinen and N. Zheng, *Nat. Commun.*, 2013, **4**, 3422–3428.
19 N. Goswami, A. Giri, M. S. Bootharaju, P. L. Xavier, T. Pradeep and S. K. Pal, *Anal. Chem.*, 2011, **83**, 9676–9680.
20 S.-I. Tanaka, J. Miyazaki, D. K. Tiwari, T. Jin and Y. Inouye, *Angew. Chem., Int. Ed.*, 2011, **50**, 431–435.
21 J. Xie, Y. Zheng and J. Y. Ying, *J. Am. Chem. Soc.*, 2009, **131**, 888–889.
22 K. Chaudhari, P. L. Xavier and T. Predeep, *ACS Nano*, 2011, **5**, 8816–8827.
23 A. Baksi, P. L. Xavier, K. Chaudhari, N. Goswami, S. K. Pal and T. Pradeep, *Nanoscale*, 2013, **5**, 2009–2016.
24 C. A. J. Lin, T. Y. Yang, C. H. Lee, S. H. Huang, R. A. Sperling, M. Zanella, J. K. Li, J. L. Shen, H. H. Wang, H. I. Yeh, W. J. Parak and W. H. Chang, *ACS Nano*, 2009, **3**, 395–401.
25 M. A. H. Muhammed, P. K. Verma, S. K. Pal, A. Retnakumari, M. Koyakutty, S. Nair and T. Pradeep, *Chem. – Eur. J.*, 2010, **16**, 10103–10112.
26 Y. Pan, S. Neuss, A. Leifert, M. Fischler, F. Wen, U. Simon, G. Schmid, W. Brandau and W. Jahnen-Dechent, *Small*, 2007, **3**, 1941–1949.
27 R. Bhattacharya and P. Mukherjee, *Adv. Drug Delivery Rev.*, 2008, **60**, 1289–1306.
28 K. S. Suslick, S. B. Choe, A. A. Cichowlas and M. W. Grinstaff, *Nature*, 1991, **353**, 414–416.
29 T. Ling, L. Xie, J. Zhu, H. Yu, H. Ye, R. Yu, Z. Cheng, L. Liu, G. Yang, Z. Cheng, Y. Wang and X. Ma, *Nano Lett.*, 2009, **9**, 1572–1576.
30 L.-M. Lacroix, S. b. Lachaize, A. Falqui, M. Respaud and B. Chaudret, *J. Am. Chem. Soc.*, 2008, **131**, 549–557.
31 L. Guo, Q. Huang, X.-y. Li and S. Yang, *Phys. Chem. Chem. Phys.*, 2001, **3**, 1661–1665.
32 B. H. Weiller, P. S. Bechthold, E. K. Parks, L. G. Pobo and S. J. Riley, *J. Chem. Phys.*, 1989, **91**, 4714–4727.
33 S. C. Richtsmeier, E. K. Parks, K. Liu, L. G. Pobo and S. J. Riley, *J. Chem. Phys.*, 1985, **82**, 3659–3665.
34 A. W. Castleman, Jr. and R. G. Keesee, *Annu. Rev. Phys. Chem.*, 1986, **37**, 525–550.
35 D. B. Jacobson and B. S. Freiser, *J. Am. Chem. Soc.*, 1984, **106**, 4623–4624.
36 H. Qian, M. Zhu, Z. Wu and R. Jin, *Acc. Chem. Res.*, 2012, **45**, 1470–1479.
37 P. Ramasamy, S. Guha, E. S. Shibu, T. S. Sreeprasad, S. Bag, A. Banerjee and T. Pradeep, *J. Mater. Chem.*, 2009, **19**, 8456–8462.
38 A. L. Rose and T. D. Waite, *Anal. Chem.*, 2001, **73**, 5909–5920.
39 T. Udayabhaskararao, Y. Sun, N. Goswami, S. K. Pal, K. Balasubramanian and T. Pradeep, *Angew. Chem., Int. Ed.*, 2012, **51**, 2155–2159.
40 J. B. Tracy, M. C. Crowe, J. F. Parker, O. Hampe, C. A. Fields-Zinna, A. Dass and R. W. Murray, *J. Am. Chem. Soc.*, 2007, **129**, 16209–16215.
41 J. Zheng, J. T. Petty and R. M. Dickson, *J. Am. Chem. Soc.*, 2003, **125**, 7780–7781.
42 J. Kříž, J. i. Dybal, E. Makrlík, J. Budka and P. Vaňura, *J. Phys. Chem. A*, 2009, **113**, 5896–5905.